Journal of Quantitative Spectroscopy & Radiative Transfer 271 (2021) 107703

Contents lists available at ScienceDirect

Journal of Quantitative Spectroscopy & Radiative Transfer

journal homepage: www.elsevier.com/locate/jqsrt

Experimental transition probabilities and oscillator strengths of doubly ionised krypton in the ultraviolet region

Maria Teresa Belmonte[a,*], Lazar Gavanski[b], Stevica Djurović[b], Santiago Mar[a], Juan Antonio Aparicio[a]

[a] Universidad de Valladolid, Departamento de Física Teórica, Atómica y Óptica, Paseo de Belén 7, 47011 Valladolid, Spain
[b] University of Novi Sad, Faculty of Sciences, Department of Physics, Trg Dositeja Obradovića 4, 21000 Novi Sad, Serbia

ARTICLE INFO

Article history:
Received 4 November 2020
Revised 27 March 2021
Accepted 30 March 2021
Available online 28 April 2021

Keywords:
Atomic emission spectroscopy
Experimental transition probabilities
Experimental oscillator strengths
Plasma diagnostics

ABSTRACT

We report 62 new experimentally obtained transition probabilities (oscillator strengths) for doubly ionized krypton within the ultraviolet wavelength region (213 – 362) nm. The transition probabilities were obtained combining measured intensities of spectral lines emitted by a plasma generated in a low-pressure pulsed arc with theoretical oscillator strengths of 12 lines used as a reference. The plasma temperature ranged from 26,200 to 29,200 K and the electron density was in the range $(1.7-3.2)\times10^{22}$ m^{-3}.

1. Introduction

Krypton (Z=36) is of great importance as an inert working gas in spectral lamps [1], lasers [2], and in fusion plasmas [3], where impurities of noble gases such as neon, argon and krypton provide transitions used for plasma diagnostics [4]. In astronomy, krypton has been identified in spectra of a variety of astronomical environments such as stellar atmospheres [5], planetary nebula [6–8], interestellar medium [9], solar wind [10] and white dwarfs [11].

Knowledge of accurate transition probabilities is vital for the diagnostics of laboratory and astrophysical plasmas and for plasma modelling. These parameters can be used for the analysis of the physical conditions (temperature, electron density, chemical composition) of objects emitting or absorbing radiation. In astrophysics, atomic transition probabilities (oscillator strengths or log(gf)) are essential to analyse and interpret astronomical spectra and to determine the chemical abundances of the different elements present [12].

However, the atomic data available is insuffient to address the current needs both in quantity and quality. In astronomy, for example, theoretically calculated transition probabilities do not have the accuracy needed to analyse high-resolution astronomical spectra [13] and experimental spectroscopy requires manpower and time, which limits the quantity of data that can be produced. This gap between "needs" and "available data" is expected to increase even further with the development of new telescopes of higher resolution over the next few years. Therefore, new accurate experimental transition probabilities are of great importance for the astronomical community.

The latest compilation of energy levels and observed spectral lines of doubly ionised krypton (Kr III) is that one of Saloman [14]. Amongst the experimental studies used in Saloman [14], the most recent work in Kr III corresponds to that of Bredice et al. [15], Reyna Almandos et al. [16], Raineri et al. [17]. These three papers are based on photographic spectra between 24 and 870 nm recorded in Lund (Sweden) for the vacuum ultraviolet region and in La Plata (Argentina) using as light sources a theta-pinch discharge and a capillary pulsed discharge, respectively [16]. The compilation of Saloman [14] does not provide transition probabilities for the spectral lines included. It can be seen how, despite the importance of krypton in many different fields, there is a lack of transition probability data for Kr III. None of the 396 lines of Kr III included in the National Institute of Standards and Technology (NIST) Atomic Spectra Database (ASD) [18] in the spectral region of this study (from 213 to 362 nm) has an absolute experimental value of transition probability. The Kurucz's Database [19], another of the databases widely used due to its extensive quantity of semi-empirical values of oscillator strengths, does not contain any data for Kr III. Values of eight relative experimental transition probabilities between 302 and 351 nm are given in Djeniže et al. [20] and lifetime measurements can be found in Fink et al. [21], Coetzer

* Corresponding author.
E-mail address: mariateresa.belmonte@uva.es (M.T. Belmonte).

https://doi.org/10.1016/j.jqsrt.2021.107703

et al. [22], Langhans et al. [23]. Theoretical oscillator strengths in the spectral region of interest were calculated by Raineri et al. [17]. These oscillator strengths were obtained from fitted values of the energy parameters using a multiconfigurational relativistic Hartree-Fock approach [17].

Due to the absence of experimental transition probabilities for Kr III in the spectral region under study, we have used the theoretical oscillator strengths of Raineri et al. [17] (converted to transition probabilities) to derive the excitation temperature of our plasma source. This temperature is then used to establish an absolute scale which allows us to obtain absolute transition probabilities from the relative intensities of spectral lines measured in this experiment.

This work is the continuation of the research carried out by our group regarding the measurement of transition probabilities in krypton. It belongs to a project spanning over more than 30 years that focuses on the study of noble gases through spectroscopy and aimes at completing and improving the accuracy of atomic transition probabilities and Stark widths. In previous articles we reported experimental transition probabilities for singly ionised krypton (Kr II) in the visible [24–26] and ultraviolet spectral regions [27]. This article completes the previous work extending our measurements to doubly ionised krypton (Kr III) in the ultraviolet. We provide 62 new experimental transition probabilities of Kr III spectral lines in the spectral range 213 – 362 nm. We measured relative intensities of Kr III spectral lines obtained in a low-pressure arc plasma. The excitation temperature, within 26,200 – 29,200 K, was determined by using the Boltzmann plot technique. We used a two-wavelength interferometric method to determine the electron density, which was in the range of $(1.7 - 3.2) \times 10^{22}$ m^{-3}.

2. Experiment and plasma diagnostics

We used a low-pressure pulsed arc plasma as the light source to measure the intensity of Kr III spectral lines. The plasma was produced in a Pyrex glass tube by discharging a 20 μF capacitor bank charged up to 7.8 kV. The tube is 175 mm in length and 19 mm in diameter. Krypton at the pressure of 120 Pa was flowing continuously through the discharge tube. The life of the plasma pulses was about 200 μs. The low pressure of the gas inside the discharge tube ensures a small self-absorption effect, except for the strongest spectral lines. Self-absorption was checked by means of a mirror placed behind the discharge tube for every spectral line in consideration. In order to ensure plasma reproducibility, the discharge tube was pre-ionized by a continuous current of several mA. More detailed descriptions of the experimental set-up can be found in Gigosos et al. [28] and Del Val et al. [29].

The spectroscopic measurements were performed end-on, 2 mm sideways from the discharge tube axis [29]. The light was led through two 3 mm diaphragms and a concave mirror (150 mm focal length) to the entrance slit of a 1.5 m Jobin-Yvon monochromator with a 2400 lines/mm UV holographic grating. A slit width of 35 m was used to obtain the best compromise between intensity and resolution. As a detector, we used an intensified charge coupled device camera ICCD 4 Quick E S20 placed at the exit plane of the monochromator. The spectral dispersion of the system spectrometer-ICCD was about 3 pm per ICCD channel [30] in the wavelength region considered in this experiment. The spectra were recorded at the instants of 50, 60, 100 and 110 μs after the beginning of the discharge. Each spectrum covered a spectral range of 3 nm. For each instant, 10 different runs were recorded, three with and seven without the self-absorption control mirror. These multiple measurements allowed us to average seven different spectra in order to increase the signal-to-noise ratio. The statistical deviation between different runs is below 5% in more than 95% of the measured spectra, which confirms the good repeatability of the different discharges. The exposure time, between 2 and 5 μs, was adjusted to obtain a high signal-to-noise ratio while avoiding saturation in the ICCD camera. In this experiment we only observed Kr II and Kr III spectral lines and recorded them in first order of diffraction. An example of a recorded spectrum, Fig. 1, shows how the Kr III lines under study were clear and well defined.

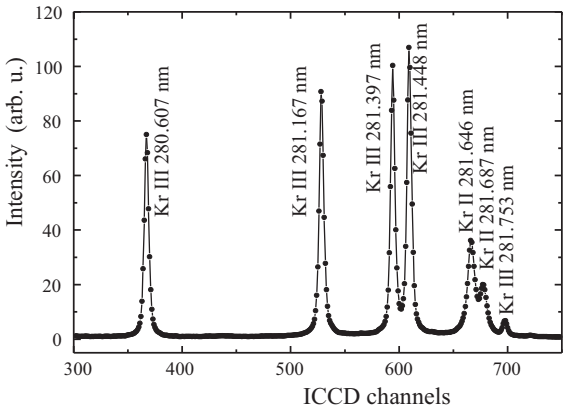

Fig. 1. Part of a recorded spectrum of doubly ionized krypton, 50 μs after the beginning of the discharge.

To determine the plasma electron density we used a two-wavelength interferometric technique with two laser beams of 543.5 nm and 632.8 nm, respectively. The discharge tube was placed in one of the arms of a Michelson interferometer with a Twyman-Green configuration. This two-wavelength interferometric method enabled us to determine the electron density by eliminating the impact of heavy particles on the refractivity index [31]. The interferometric channel was 2 mm off the discharge tube axis, opposite the spectroscopic channel. The plasma has high-axial homogeneity and very good cylindrical symmetry [29], which allowed for simultaneous spectroscopic and interferometric measurements. The measured electron density was in the range $(1.7 - 3.2) \times 10^{22}$ m^{-3}. The estimated experimental error is between 5 and 10%.

We used the Boltzmann analysis to determine the excitation temperature of our plasma light source. If the plasma is known to be in at least partial local thermodynamic equilibrium (pLTE), the population of the energy levels within the range of study will follow the Boltzmann distribution. This allows us to express the intensity of a spectral line (total number of photons involved in a particular transition) as:

$$I_{ul} = \beta \frac{g_u A_{ul}}{\lambda_{ul}} e^{\frac{E_u}{kT}} \quad (1)$$

where u and l refer to upper and lower energy level, I_{ul} is the intensity of the spectral line, β is a constant, g_u is the statistical weight of the upper energy level, A_{ul} is the absolute transition probability, λ_{ul} is the transition wavelength, E_u is the upper energy level, k is the Boltzmann constant and T is the temperature. The least-squares linear fit to $\ln(I_{ul}\lambda_{ul}/g_u A_{ul})$ versus E_u is known as the Boltzmann plot. The area under the line profile is considered as a relative line intensity and is used to obtain the Boltzmann plots, as well as for the derivation of new transition probabilities.

In order to use the Boltzmann plot technique, two critical aspects must be considered in addition to accurate measurements of spectral line intensities. On the one hand, it is necessary to find in the bibliography a reliable set of transition probabilities for some of the measured spectral lines. We will refer to these lines as the "reference lines" (A_{ref}). The case of Kr III is problematic given the lack of experimental transition probabilities available, as there are only theoretically calculated oscillator strengths from Raineri et al.

Table 1
Selected spectral lines used as a set of reference lines. The upper energy levels, E_u, and statistical weights for the upper energy levels, g_u, were taken from Kramida et al. [18]. Transition probabilities were calculated using Eq. (2) from the oscillator strengths given in Raineri et al. [17].

Wavelength (nm)	E_u (eV)	g_u	A_{Ref} (10^8) s($^{-1}$)
213.870	24.236	7	0.1415
221.560	24.035	5	0.1115
281.167	24.651	3	0.5651
290.917	22.327	5	0.1785
309.716	22.327	5	0.2324
312.246	26.317	3	0.8129
315.175	25.852	5	0.2427
322.062	25.948	3	1.2222
322.224	25.948	3	0.4118
327.165	22.271	3	0.3668
344.871	25.695	3	0.6063
351.455	25.156	5	0.2763

[17]. After a careful analysis, we selected a set of 12 lines (Table 1) coming from upper energy levels in the range from 22 to 27 eV for which we obtained a Boltzmann plot of reasonable linearity ($R^2 > 0.8$). Since the temperature is obtained from the slope of the linear fitting, an error of a constant factor (i.e., some systematic error) would not change the value of the temperature. We converted the $\log(g_l f_{lu})$ from Raineri et al. [17] into transition probabilities A_{ul} using the following expression from Thorne et al. [32]:

$$\log(g_l f_{lu}) = \log(A_{ul} g_u \lambda_{ul}^2 \times 1.499 \times 10^{-14}) \quad (2)$$

where g_l and g_u are the statistical weights of the lower and upper energy levels, respectively, f_{lu} is the oscillator strength and λ_{ul} is the wavelength of the emission spectral line expressed in nm. It is important to notice that the oscillator strength, f_{lu}, is a quantity defined for absorption, whereas transition probability, A_{ul}, is defined for emission. The quantity provided in many papers due to its convenience for astronomers is the decimal logarithm of the oscillator strength weigthed by the statistical weigth of the lower energy level of the transition, $\log(g_l f_{lu})$.

On the other hand, to use the Boltzmann plot technique the plasma source has to fulfill the conditions for at least partial local thermodynamic equilibrium (pLTE). According to strict criteria from Griem [33] and McWhirter [34], our plasma is not in pLTE. If another criterion is used, as suggested in Travaillé et al. [35], the equilibrium conditions are satisfied. The linearity of the Boltzmann plots across the 5 eV upper energy range ($R^2 > 0.8$) supports the pLTE conditions for lines coming from energy levels from 22 to 27 eV. We obtained the plasma temperature for four different instants of the life of the plasma (50, 60, 100 and 110 μs), which were 29,187, 28,721, 26,250 and 27,535 K, respectively. The uncertainty of the temperature ranged between 5–10%.

3. Data analysis and determination of transition probabilities

Before using the experimental intensities (area under the profile) of spectral lines to determine both the excitation temperature and the transition probabilities, it is necessary to intensity calibrate all the recorded spectra using the spectral response function of the experimental set-up to eliminate any wavelength dependence introduced by the optics, monochromator or the ICCD camera. We used a calibrated deuterium lamp (L202 Hamamatsu) to obtain the response function for the whole ultraviolet (UV) spectral region of interest. The deuterium lamp was placed between the pulsed discharge lamp and the entrance slit of the spectrometer and carefully aligned so that the light path was the same as that one followed by the light leaving the pulsed lamp. All the spectra were recorded using the continuous mode of the ICCD camera. The monochromator was tuned between 200 and 370 nm at 5 nm intervals. For each tuning wavelength between 50 and 100 spectra, depending on the intensity of the lamp, were accumulated to reduce the noise. A background spectrum was recorded at the beginning and the end of every set of calibration measurements and subtracted from each of the calibration spectra in order to remove the electrical noise and the background light. The uncertainty of the response function was estimated to be lower than 4%. The contributions to this uncertainty are the calibration data and the statistical uncertainties of the different measurements.

In order to determine spectral line intensities, we fitted each of the 3 nm intensity-corrected spectra to a sum of a linear background to account for the continuum emission and a lorentzian function per emission line. The deviation between the fitted function and the experimental profiles was always lower than 3%. The experimental conditions of this work (high electron densities) ensure that the broadening of the recorded spectral lines comes primarily from the Stark effect, which has a lorentzian profile. The details can be found in Djurović et al. [36].

3.1. Determination of transition probabilities

We used the relative intensity of the recorded spectral lines to determine the transition probabilities. Using Eq. (1), we can write the ratio between the intensities of a spectral line with a known value of transition probability (reference line) and a line with an unknown value of transition probability (line under study). Rearranging that expression, we can derived the unknown transition probability in absolute units as:

$$A_{ul} = A_{ref} \frac{I_{ul}}{I_{ref}} \frac{\lambda_{ul}}{\lambda_{ref}} \frac{g_{ref}}{g_u} e^{\frac{E_u - E_{ref}}{kT}} \quad (3)$$

where the subindexes ref and ul refer to the reference line and the line under study, respectively. In the previous equation A is the absolute transition probability, I_{ul} is the relative line intensity, λ is the wavelength, E_{ul} and g_u are the energy and the statistical weight of the upper energy level, respectively, k is the Boltzmann constant and T is the temperature.

We used as reference data the same theoretical oscillator strengths from Raineri et al. [17] previously used for the determination of the excitation temperature (see A_{ref} in Table 1). It is worth remembering that this set of 12 reference lines was carefully selected amongst Raineri et al. [17] values. Using Eq. (3), we obtained a set of 48 individual values of A_{ul} for each spectral line under study using intensities of each of the reference lines for each of the four different instants of the plasma life.

The final value of the transition probability, $\bar{A}$, was calculated using Eq. (4) as a weighted arithmetic mean of the 48 values. Here, we introduce a change of notation for convenience when writing this equation. We remove the subscript ul used previously in A_{ul} and refer to every individual value of transition probabily as A_{rt}, where r refers to the reference line used to calculate it and t to the instant of the plasma life.

$$\bar{A} = \frac{\sum_{r=1}^{n_r} \sum_{t=1}^{n_t} \omega_{rt} A_{rt}}{\sum_{r=1}^{n_r} \sum_{t=1}^{n_t} \omega_{rt}} \quad (4)$$

where n_r is the number of reference lines used, n_t is the number of instants of measurement (in our case 12 and 4, respectively) and ω_{rt} is the weight associated to the value A_{rt} calculated as:

$$\omega_{rt} = \frac{1}{(\Delta A_{rt})^2} \quad (5)$$

with ΔA_{rt} being the uncertainty introduced by our measurement in every individual transition probability obtained with a given reference line, r, and for a given instant, t, of the plasma life. The

calculation of this uncertainty is explained in Section 3.2. We removed from the weighted mean any value differing from it more than 2σ.

3.2. Calculation of uncertainties

The transition probability uncertainties included in Table 2 were calculated as the error of the weigthed mean, $\Delta\bar{A}$, using equation 4.19 from Bevington and Robinson [37]:

$$\Delta\bar{A} = \frac{1}{\sqrt{\sum_{r=1}^{n_r}\sum_{t=1}^{n_t}\omega_{rt}}} \tag{6}$$

To calculate this uncertainty and making used of Eq. (5), it is necessary to evaluate the uncertainty of each of the values ΔA_{rt}. From Eq. (3), we see that A_{rt} can be written as a function of the intensity of the line under study (I_{st}), the intensity of the reference line (I_{rt}), the temperature (T) and the transition probability of the reference line (A_{ref}):

$$A_{rt} = f(I_{st}, I_{rt}, T_t, A_{ref}) \tag{7}$$

Our measurement procedure introduces uncertainty in the intensities and the temperatures. Regarding the uncertainty of the transition probabilities of the reference lines, ΔA_{ref}, these values are not given by Raineri et al. [17]. We are therefore providing the relative uncertainties introduced by our measurements.

From Eq. (7), assuming that the uncertainties of I_{st}, I_{rt} and T_t are not correlated [38], we can apply the law of the propagation of uncertainty as:

$$(\Delta A_{rt})^2 = \left(\frac{\partial A_{rt}}{\partial I_{st}}\right)^2 (\Delta I_{st})^2 + \left(\frac{\partial A_{rt}}{\partial I_{rt}}\right)^2 (\Delta I_{rt})^2 + \left(\frac{\partial A_{rt}}{\partial T_t}\right)^2 (\Delta T_t)^2 \tag{8}$$

where ΔA_{rt} is the uncertainty associated with the transition probability we are calculating, ΔI_{st}, ΔI_{rt} are the uncertainties of the intensities of the line under study and the reference line, respectively, and ΔT_t is the uncertainty of the temperature obtained in the Boltzmann plot. As mentioned in Sikstrom et al. [38], we are using the term standard uncertainty according to the definition given in Taylor and Kuyatt [39], i.e. equal to the positive square root of the estimated variance $(\Delta A_{rt})^2$.

3.2.1. Uncertainty attributed to the line intensity.

The uncertainty of the line intensity was calculated taking into account the following contributions:

* **Calibration uncertainty** (σ_{calib}): as previously explained in Section 3, the uncertainty of the response curve as a function of either the wavelength or the detector channel is estimated to be $< 4\%$.
* **Fitting uncertainty** (σ): ratio between the standard deviation of the residuals (SD) when fitting a line on an interval equal to the full width at half maximum (FWHM) and the maximum height of the line (I_c). It is $< 3\%$ for the lines in this study.

$$\sigma = \frac{SD}{I_c} \tag{9}$$

* **Background-peak** (BP): ratio between the background intensity (B) and the maximum height of the line (I_c).

$$BP = \frac{B}{I_c} \tag{10}$$

* **Self-absorption coefficient of the spectral lines** (SA): this is the fraction of the original profile that is necessary to add in order to reconstruct the spectral line of interest.

$$SA = \frac{I_c - I_o}{I_c} \tag{11}$$

where I_o (original value) is the measured peak intensity and I_c (corrected value) is the reconstructed peak intensity. We have excluded from our results all the lines for which $SA > 0.1$.

* **Overlapping with the adjacent left** (O_l) or right (O_r)**line**: this quantity is given by the expression:

$$O_i = \frac{\omega + \omega_i}{d_i}\frac{I_i}{I_c} \tag{12}$$

where i represents left (l) or right (r), ω and ω_i are the half FWHM of the line under study and the adjacent line, respectively, and d_i is the distance between the peaks of the line under study and the adjacent one. The second factor contains the ratio between the intensity of the adjacent line (I_i) and the intensity of the studied line (I_c).

All the previous factors contribute to the final uncertainty of the intensity in different ways. After analyzing hundreds of spectra, we arrived at the empirical expression for the relative uncertainty of the intensity:

$$\frac{\Delta I}{I} = \sqrt{\sigma_{calib}^2 + \sigma^2 + \left(\frac{BP}{2}\right)^2 + (2(SA)^2)^2 + \left(\frac{O_L}{20}\right)^2 + \left(\frac{O_R}{20}\right)^2} \tag{13}$$

This equation has been tested in a wide range of situations (self-absorbed lines, overlapping lines with similar and different intensities, singly and doubly ionized atoms) and we find that it provides very reasonable uncertainties in the majority of cases.

For the lines included in this article, the uncertainty introduced by our measurements in the intensity is $< 8\%$. The improvement in the calculation of uncertainties is an ongoing project in our group. A full treatment of uncertainties using rigurous statistical theory (covariance matrix) has been recently developed and implemented and will be described in our next work.

3.2.2. Uncertainty attributed to the temperature.

The uncertainty of the temperature was calculated from the uncertainty of the slope of a non-weigthed linear fit of the Boltzmann plot including the 12 reference lines from Table 1. This uncertainty ranged between 5–10%.

4. Results and discussion

The results of 62 new values of Kr III transition probabilities for lines coming from energy levels between 22 and 27 eV are given in Table 2 ordered in ascending wavelength. The first column of Table 2 contains the wavelengths in nm. The second and third columns contain the values of the upper and lower energy levels of the corresponding transition expressed in eV. The next six columns contain configurations, terms and total angular momentum J for the upper and lower energy levels. All these data are taken from Kramida et al. [18]. The next two columns include our new measured transition probabilities, A_{TW}, and their estimated relative uncertainty in percentage obtained as explained in Section 3.2. We want to emphasize that these relative uncertainties only take into account the errors introduced by our experimental procedure. They do not account for the uncertainty of the transition probabilities used as a reference, A_{ref}, since Raineri et al. [17] did not provide these values. Columns 12^{th} and 13^{th} include our results expressed as $\log(g_l f_{lu})$, with the uncertainty in dex (x dex = 10^x). The last column of Table 2 contains the ratio between the transition probabilites from Raineri et al. [17] and those from this work.

Fig. 2 shows the Boltzmann plot obtained using our new transition probability data and intensities corresponding to those 50 μs after the beginning of the discharge. The linearity of this Boltzmann plot ($R^2 = 0.97$) illustrates the consistency of our new A_{TW} data and the measured spectral line intensities. Given the lack of

Table 2
Experimental values of Kr III transition probabilities from this work, A_{TW}, and the corresponding value of $\log(g_l f_{lu})$. The last column includes the comparison between the theoretical transition probabilities from Raineri et al. [17], A_{RAI}, and those from this work as A_{RAI}/A_{TW}.

λ_{ul} (nm)	E_u (eV)	E_l (eV)	Upper Conf.	Term	J_u	Lower Conf.	Term	J_l	A_{TW} (10^8 s^{-1})	Unc. (%)	$\log(g_l f_{lu})$	Unc. (dex)	A_{RAI}/A_{TW}
213.870	24.236	18.440	$(^2D^o)5p$	^{3}D	3	$(^4S^o)4d$	$^3D^o$	3	0.1135	6	-1.26	0.03	1.25
221.560	24.035	18.440	$(^2D^o)5p$	^3D	2	$(^4S^o)4d$	$^3D^o$	3	0.1034	6	-1.42	0.03	1.08
227.376	23.892	18.440	$(^2D^o)5p$	^3F	2	$(^4S^o)4d$	$^3D^o$	3	0.0613	7	-1.62	0.03	3.33
230.300	24.562	19.180	$(^2D^o)5p$	^3P	2	$(^2D^o)4d$	$^3F^o$	3	0.0558	7	-1.65	0.03	1.33
240.010	23.647	18.483	$(^2D^o)5p$	^3D	1	$(^4S^o)4d$	$^3D^o$	1	0.1380	6	-1.45	0.03	1.39
246.276	26.416	21.383	$(^2P^o)5p$	^3P	2	$(^2D^o)4d$	$^3D^o$	2	0.0347	14	-1.80	0.06	1.32
250.064	26.721	21.765	$(^4S^o)6s$	$^5S^o$	2	$(^4S^o)5p$	^5p	1	1.2133	6	-0.25	0.03	1.22
251.542	26.721	21.794	$(^4S^o)6s$	$^5S^o$	2	$(^4S^o)5p$	^5p	2	1.9836	6	-0.03	0.03	1.22
257.119	24.172	19.352	$(^2D^o)5p$	^1F	3	$(^2D^o)4d$	$^3F^o$	4	0.2713	6	-0.73	0.03	1.08
258.947	26.416	21.629	$(^2P^o)5p$	^3P	2	$(^2D^o)4d$	$^3D^o$	3	0.2390	9	-0.92	0.04	1.45
260.435	25.948	21.189	$(^2P^o)5p$	^3P	1	$(^2D^o)5s$	$^1D^o$	2	1.2376	6	-0.42	0.03	0.38
261.519	26.416	21.676	$(^2P^o)5p$	^3P	2	$(^2P^o)4d$	$^3F^o$	3	0.1619	6	-1.08	0.03	0.31
262.311	24.562	19.837	$(^2D^o)5p$	^3P	2	$(^2D^o)4d$	$^3G^o$	3	0.0469	30	-1.62	0.12	0.07
264.174	25.156	20.464	$(^2D^o)5p$	^1D	2	$(^2D^o)5s$	$^3D^o$	3	0.0936	6	-1.31	0.03	0.98
265.366	26.300	21.629	$(^2P^o)5p$	^1D	2	$(^2D^o)4d$	$^3D^o$	3	0.1643	6	-1.06	0.03	0.78
265.800	25.852	21.189	$(^2P^o)5p$	^3D	2	$(^2D^o)5s$	$^1D^o$	2	0.0574	7	-1.52	0.03	0.93
269.807	26.317	21.723	$(^2P^o)5p$	^1P	1	$(^2P^o)4d$	$^3F^o$	2	0.2819	18	-1.04	0.07	0.98
271.519	25.948	21.383	$(^2P^o)5p$	^3P	1	$(^2D^o)4d$	$^3D^o$	2	0.4654	6	-0.81	0.03	1.16
273.041	25.864	21.325	$(^2D^o)5p$	^3S	1	$(^2P^o)4d$	$^3P^o$	0	0.1931	6	-1.19	0.03	1.45
274.303	26.846	22.327	$(^4S^o)5d$	$^5D^o$	2	$(^4S^o)5p$	^3P	2	0.0806	12	-1.34	0.05	1.39
274.405	26.844	22.327	$(^4S^o)5d$	$^5D^o$	1	$(^4S^o)5p$	^3P	2	0.0685	9	-1.64	0.04	0.80
276.590	25.864	21.383	$(^2D^o)5p$	^3S	1	$(^2D^o)4d$	$^3D^o$	2	0.0145	15	-2.30	0.06	1.02
280.607	25.864	21.447	$(^2D^o)5p$	^3S	1	$(^2P^o)4d$	$^3P^o$	1	0.6676	6	-0.63	0.03	1.18
281.167	24.651	20.243	$(^2D^o)5p$	^3P	1	$(^2D^o)5s$	$^3D^o$	1	0.5463	6	-0.71	0.03	1.03
282.095	26.721	22.327	$(^4S^o)6s$	$^5S^o$	2	$(^4S^o)5p$	^3P	2	0.1068	6	-1.20	0.03	0.20
282.941	26.300	21.919	$(^2P^o)5p$	^1D	2	$(^2P^o)4d$	$^3P^o$	2	0.1759	6	-0.98	0.03	0.87
283.594	25.695	21.325	$(^2P^o)5p$	^3D	1	$(^2P^o)4d$	$^3P^o$	0	0.2732	6	-1.01	0.03	1.10
285.116	24.236	19.889	$(^2D^o)5p$	^3D	3	$(^2D^o)4d$	$^3G^o$	4	0.3643	6	-0.51	0.03	1.49
285.322	26.020	21.676	$(^2P^o)5p$	^3D	3	$(^2P^o)4d$	$^3F^o$	3	0.0132	8	-1.95	0.03	2.27
285.905	24.172	19.837	$(^2D^o)5p$	^1F	3	$(^2D^o)4d$	$^3G^o$	3	0.0205	7	-1.76	0.03	0.62
288.455	26.020	21.723	$(^2P^o)5p$	^3D	3	$(^2P^o)4d$	$^3F^o$	2	0.0218	21	-1.72	0.08	1.08
290.917	22.327	18.067	$(^4S^o)5p$	^3P	2	$(^4S^o)5s$	$^5S^o$	2	0.1703	6	-0.97	0.03	1.05
304.480	24.261	20.190	$(^2D^o)5p$	^3F	4	$(^2D^o)4d$	$^1G^o$	4	0.0248	9	-1.51	0.04	0.88
309.716	22.327	18.325	$(^4S^o)5p$	^3P	2	$(^4S^o)4d$	$^3D^o$	2	0.2277	6	-0.79	0.03	1.02
312.246	26.317	22.348	$(^2P^o)5p$	^1P	1	$(^2P^o)5s$	$^3P^o$	2	0.8350	6	-0.44	0.03	0.97
313.620	26.300	22.348	$(^2P^o)5p$	^1D	2	$(^2P^o)5s$	$^3P^o$	2	0.2661	6	-0.71	0.03	0.65
315.175	25.852	21.919	$(^2P^o)5p$	^3D	2	$(^2P^o)4d$	$^3P^o$	2	0.2117	6	-0.80	0.03	1.15
317.093	26.010	22.101	$(^2P^o)5p$	^3P	0	$(^2P^o)5s$	$^3P^o$	1	2.4584	6	-0.43	0.03	1.00
322.062	25.948	22.099	$(^2P^o)5p$	^3P	1	$(^2P^o)5s$	$^3P^o$	0	1.1303	6	-0.28	0.03	1.09
322.224	25.948	22.101	$(^2P^o)5p$	^3P	1	$(^2P^o)5s$	$^3P^o$	1	0.4528	6	-0.68	0.03	0.91
322.485	26.317	22.474	$(^2P^o)5p$	^1P	1	$(^2D^o)4d$	$^3S^o$	1	0.9229	6	-0.37	0.03	0.08
324.662	26.416	22.598	$(^2P^o)5p$	^3P	2	$(^2P^o)5s$	$^1P^o$	1	0.3919	21	-0.51	0.08	1.19
327.165	22.271	18.483	$(^4S^o)5p$	^3P	1	$(^4S^o)4d$	$^3D^o$	1	0.3887	7	-0.73	0.03	0.94
327.942	24.068	20.288	$(^2D^o)5p$	^1P	1	$(^2D^o)5s$	$^3D^o$	2	0.0098	10	-2.32	0.04	1.67
328.589	24.236	20.464	$(^2D^o)5p$	^3D	3	$(^2D^o)5s$	$^3D^o$	3	0.2526	6	-0.54	0.03	1.54
329.388	25.864	22.101	$(^2D^o)5p$	^3S	1	$(^2P^o)5s$	$^3P^o$	1	0.1121	7	-1.26	0.03	1.75
334.817	26.300	22.598	$(^2P^o)5p$	^1D	2	$(^2P^o)5s$	$^1P^o$	1	0.3092	6	-0.59	0.03	5.56
338.893	24.172	20.515	$(^2D^o)5p$	^1F	3	$(^2P^o)4d$	$^1D^o$	2	0.1693	6	-0.69	0.03	0.63
339.658	23.892	20.243	$(^2D^o)5p$	^3F	2	$(^2D^o)5s$	$^3D^o$	1	0.1480	6	-0.89	0.03	12.5
342.883	26.300	22.685	$(^2P^o)5p$	^1D	2	$(^2D^o)4d$	$^1F^o$	3	0.2278	6	-0.70	0.03	1.08
344.286	25.948	22.348	$(^2P^o)5p$	^3P	1	$(^2P^o)5s$	$^3P^o$	2	0.2102	9	-0.95	0.04	1.32
344.871	25.695	22.101	$(^2P^o)5p$	^3D	1	$(^2P^o)5s$	$^3P^o$	1	0.6582	6	-0.45	0.03	0.92
347.102	24.035	20.464	$(^2D^o)5p$	^3D	2	$(^2D^o)5s$	$^3D^o$	3	0.0498	6	-1.35	0.03	4.55
349.280	24.651	21.102	$(^2D^o)5p$	^3P	1	$(^2D^o)4d$	$^3D^o$	1	0.3471	6	-0.72	0.03	1.15
351.455	25.156	21.629	$(^2D^o)5p$	^1D	2	$(^2D^o)4d$	$^3D^o$	3	0.2236	6	-0.68	0.03	1.23
352.111	24.035	20.515	$(^2D^o)5p$	^3D	2	$(^2P^o)4d$	$^1D^o$	2	0.0315	6	-1.53	0.03	8.33
353.720	25.852	22.348	$(^2P^o)5p$	^3D	2	$(^2P^o)5s$	$^3P^o$	2	0.0226	11	-1.67	0.05	0.83
354.942	26.416	22.924	$(^2P^o)5p$	^3P	2	$(^2P^o)4d$	$^3D^o$	3	0.7720	6	-0.14	0.03	1.09
356.772	25.948	22.474	$(^2P^o)5p$	^3P	1	$(^2D^o)4d$	$^3S^o$	1	0.4044	7	-0.64	0.03	0.73
357.995	24.651	21.189	$(^2D^o)5p$	^3P	1	$(^2D^o)5s$	$^1D^o$	2	0.0286	9	-1.78	0.04	1.14
361.106	25.156	21.723	$(^2D^o)5p$	^1D	2	$(^2P^o)4d$	$^3F^o$	2	0.0881	6	-1.07	0.03	0.96
361.582	23.892	20.464	$(^2D^o)5p$	^3F	2	$(^2D^o)5s$	$^3D^o$	3	0.1845	6	-0.74	0.03	0.25

good quality experimental A_{ul}-values to set an absolute scale, we only include results for clean, intense Kr III spectral lines. For these lines, the error introduced by our measurements is normally lower than 10%. Out of the 200 spectral lines fitted in this experiment, we selected 87 lines with good clean profiles and with non or very small self-absorption. From those lines, we did a second selection and chose lines that lay strictly within the upper energy level range of the reference lines used to calculate the temperature with the Boltzmann plot (22–27 eV). The 62 lines included in this work represent a 30% of all the lines measured.

We have compared our results with the only transition probabilities available in the literature, those obtained from the theoretical oscillator strengths of Raineri et al. [17]. In Fig. 3 we plot the ratio between the transition probabilities from Raineri et al.

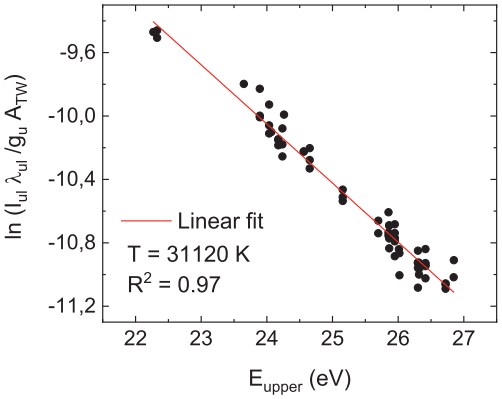

Fig. 2. Boltzmann plot obtained using the 62 spectral lines in Table 2 and our new values of transition probability, A_{TW}. The intensities used correspond to those 50 μs after the beginning of the discharge.

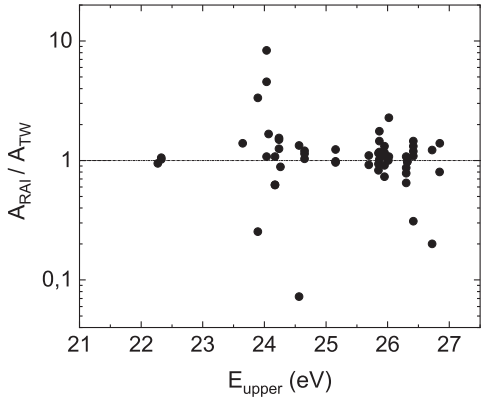

Fig. 3. Comparison between the transition probabilities from Raineri et al. [17], A_{RAI}, and those from this work, A_{TW}, as a function of the upper energy level.

[17] and our values versus the upper energy level of the transition for spectral lines coming from levels between 22 and 27 eV. It should be noticed than only 12 out of the 62 lines plotted in Fig. 3 were used as an absolute reference. This set of 12 lines was carefully selected after a laborious process to obtain a set of good lines based on the linearity of the Boltzmann plot. The assumption of pLTE has already been tested for a krypton plasma in Belmonte et al. [27] where experimental A_{ul}-values for Kr II were available. This careful process of selection of the reference lines minimizes the problems derivated from for the lack of good experimental A_{ul}-values for Kr III to use as a reference.

To further check the consistency of our results, we have followed the approach of Curry [40] of combining observed intensities from an author with transition probabilities from another one. This approach could be a useful way of obtaining transition probabilities for lines which were not measured in our experiment using intensities from previous studies. The intensities provided in the ASD database [18] for the 62 spectral lines that appear in Table 2 are those from the compilation of Saloman [14] and come from the work of Humphreys [41]. From them, we chose 23 lines for which the intensities in Humphreys [41] are bigger than 10 as lines with smaller intensities yielded Boltzmann plots with regression coeffients of around 0.11. We obtained two different Boltzmann plots combining the intensities from Humphreys [41] with either our new transition probabilities A_{TW} (upper panel in Fig. 4) or those from Raineri et al. [17] A_{RAI} (lower panel in Fig. 4). As stated in Cowley [42], in making the previous Bolzmann plots we are proceeding on a "purely empirical basis without becoming involved in more fundamental questions such as the existence of a

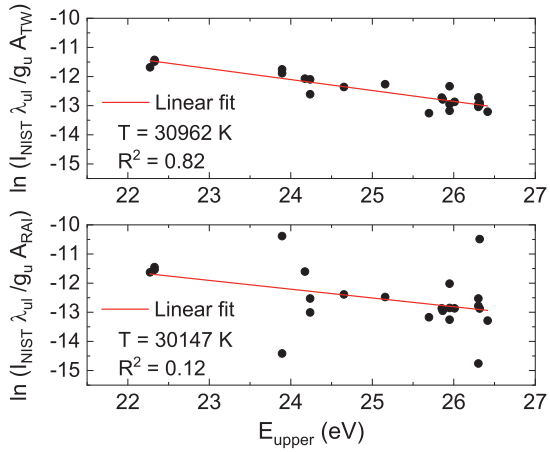

Fig. 4. Boltzmann plots for 23 lines of Kr III using the observed intensities from Humphreys [41] and the transition probabilities from this work (A_{TW}, upper panel) and from Raineri et al. [17] (A_{RAI}, lower panel).

Boltzmann distribution of energy levels" in the Geissler tube discharge used by Humphreys [41].

The upper panel in Fig. 4 shows a reasonable linearity of the Boltzmann plot using our transition probabilities within the range of upper energy levels considered, with an $R^2 = 0.82$. From the least-squares linear fit of the upper panel, the temperature T and β parameter from Eq. (1) can be determined and used to obtain new values of transition probabilities for lines that were not measured in our experiment using the intensities from Humphreys [41]. This method, as mention in Cowley [42], can be convenient to use the already existing atomic data and "transform an extensive system of intensity measurements into a useful set of oscillator strengths" and can prove useful to both astrophysicists and atomic physicists for modelling applications that need a big volume of transition probabilities of reasonable accuracy [43]. It is important to bear in mind that the success of this approach depends on the accuracy of the set of transition probabilities used to obtain the β and T parameters [42]. This suports the importance of having sets of accurate transition probabilities like the one provided in this paper which, even if relatively small, will allow users to make the most of the much bigger set of intensities from older studies. This approach could prove an efficient way of obtaining moderately accurate transition probabilities when limited resources or manpower impede to take new measurements.

5. Conclusions

This paper reports 62 new experimental values of absolute transition probabilities (oscillator strengths) for spectral lines of doubly ionised Krypton (Kr III) in the ultraviolet wavelength region 213 – 362 nm. The lines studied correspond to 4d – 5p, 5s – 5p, 5p – 5d, 5p – 6s and 5p – 6d transitions, with upper energy levels ranging from 22 to 27 eV. As a light source, we used a low-pressure arc lamp designed and made in-house. We obtained the new transition probabilities from measured relative line intensities that we converted to absolute units using the theoretical oscillator strengths from [17]. The uncertainties of the transition probabilities introduced by our measurements are lower than 10% for 53 out of the 62 values. The results presented in this work provide a new set of accurate experimental data which could also be used to obtain transition probabilities for Kr III lines not recorded in this experiment using the intensities available in the ASD database [18]. This approach could be useful for uses that require data of reasonable accuracy for a large number of spectral lines.

Declaration of Competing Interest

The authors declare that they have no known competing financial interests or personal relationships that could have appeared to influence the work reported in this paper.

CRediT authorship contribution statement

Maria Teresa Belmonte: Writing - original draft, Writing - review & editing, Conceptualization, Formal analysis. **Lazar Gavanski:** Formal analysis, Writing - review & editing. **Stevica Djurović:** Funding acquisition, Conceptualization, Investigation, Writing - review & editing. **Santiago Mar:** Funding acquisition, Conceptualization, Investigation, Writing - review & editing. **Juan Antonio Aparicio:** Investigation, Conceptualization.

Acknowledgments

M. T. Belmonte acknowledges financial support from the University of Valladolid (Spain) through the FPI PhD grant. L. Gavanski and S. Djurović thanks the Ministry of Education, Science and Technological development of Republic Serbia for support under Grant No. 451-03-68/2020-14/200125. The authors would like to thank the referee for the very useful comments during the review process.

Dr Juan Antonio Aparicio ("Apa") passed away during the revision of this manuscript after a long illness. The other authors want to acknowledge his guidance throughout the process of this research which, beside the current manuscript, involved many other papers. He had a leading role at the beginning of this project providing original ideas, setting-up the experiment and helping with the analysis of the data. His thoughtful comments on this manuscript until his last days were crucial for the success of the present work.

References

[1] Cayless MA, Marsden AM. Lamps and lighting, 3rd edn. Edward Arnold, London; 1983.
[2] Shimoda K. Introduction to laser physics. Springer Series in Optical Sciences; 1984.
[3] Loch SD, Pindzola MS, Ballance CP, Griffin DC, Mitnik DM, Badnell NR, O'Mullane MG, Summers HP, Whiteford AD. Electron-impact ionization of all ionization stages of krypton. Physical Review A - Atomic, Molecular, and Optical Physics 2002;66(5):7. doi:10.1103/PhysRevA.66.052708.
[4] Chen H, Beiersdorfer P, Harris CL, Utter SB, Wong KL. Spectral catalog of kr optical lines for the development of diagnostics for fusion plasmas. Rev Sci Instrum 2001;72:983–6. doi:10.1063/1.1319604.
[5] Bidelman WP. ApJ 1962(67):111.
[6] Pequignot D, Baluteau JP. The identification of krypton, xenon, and other elements of rows 4, 5, and 6 of the periodic table in the planetary nebula NGC 7027. Astronomy & Astrophysics 1994;283:593–625.
[7] Dinerstein HL. Neutron-Capture elements in planetary nebulae: identification of two near-Infrared emission lines as kr III and se IV. Astrophys J 2002;550(2):L223–6. doi:10.1086/319645.
[8] Sterling NC. Atomic data for neutron-capture elements. Astronomy & Astrophysics 2011;533:A62. doi:10.1051/0004-6361/201117471.
[9] Cardelli JA, Meyer DM. The abundance of interstellar krypton. Astrophys J 1997;477:57–60.
[10] Morton DC. Atomic data for resonance absorption lines. II. wavelengths longward of the lyman limit for heavy elements. The Astrophysical Journal Supplement Series 2000;130(2):403–36. doi:10.1086/317349.
[11] Werner K, Rauch T, Ringat E, Kruk JW. First detection of krypton and xenon in a white dwarf. Astrophysical Journal Letters 2012;753(1):3–7. doi:10.1088/2041-8205/753/1/L7.
[12] Allende Prieto C. Solar and stellar photospheric abundances. Living Rev Sol Phys 2016;13(1):1–40. arXiv:1602.01121. doi:10.1007/s41116-016-0001-6.
[13] Barklem PS. Accurate abundance analysis of late-type stars: advances in atomic physics. Astron Astrophys Rev 2016;24(1):1–54. arXiv:1604.07659. doi:10.1007/s00159-016-0095-9.
[14] Saloman EB. Energy levels and observed spectral lines of krypton, kr i through kr XXXVI. J Phys Chem Ref Data 2007;36(1):215–86. doi:10.1063/1.2227036.
[15] Bredice F, Reyna Almandos JG, Gallardo M, Di Rocco HO, Trigueiros AG. Revised and extended analysis of the low configurations in kr III. Journal of the Optical Society of America B 1988;5(2):222–35.
[16] Reyna Almandos JG, Bredice F, Raineri M, Gallardo M, Trigueiros AG. New energy levels of the kr III spectrum. J Phys B: At Mol Opt Phys 1996;29(23):5643–50. doi:10.1088/0953-4075/29/23/010.
[17] Raineri M, Reyna Almandos JG, Bredice F, Gallardo M, Trigueiros AG, Pettersson S-G. J Quant Spectrosc Radiat Transfer 1998;60(1):25–42.
[18] Kramida A., Ralchenko Y., Reader J., and NIST ASD Team. NIST Atomic Spectra Database (ver. 5.7.1), [Online]. Available: https://physics.nist.gov/asd [2019, November 5]. National Institute of Standards and Technology, Gaithersburg, MD.; 2017.
[19] Kurucz R.L.. Kurucz database. 2020. http://kurucz.harvard.edu/atoms.html.
[20] Djeniže S, Milosavljević V, Dimitrijević MS. Transition probabilities in krII and krIII spectra. European Physical Journal D 2003;27(3):209–13. doi:10.1140/epjd/e2003-00278-2.
[21] Fink U, Bashkin S, Bickel WS. Transitions and level lifetimes in ne II, III, ar II, III, kr II, III AND xe II *. J Quant Spectrosc Radiat Transfer 1970;10:1241–56. doi:10.1016/0022-4073(70)90008-7.
[22] Coetzer FJ, Kotze PB, Kotze TC, Westhuizen PVD. Beam-foil mean lifetimes in kr III obtained from arbitrarily normalized decay curve (ANDC) analyses. Spectrochimica Acta - Part B Atomic Spectroscopy 1984;39(8):1021–4.
[23] Langhans G, Schade W, Helbig V. Lifetime measurements of the kr III 5p. Phys Lett A 1993;183:205–8.
[24] De Castro A, Aparicio JA, Del Val JA, González VR, Mar S. Measurement of stark broadening and shift constants of singly ionized krypton lines. J Phys B: At Mol Opt Phys 2001;34(16):3275–86. doi:10.1088/0953-4075/34/16/306.
[25] Rodriguez F, Aparicio JA, De Castro A, Del Val JA, Gonzalez V, Mar S. Measurement of several transition probabilities in singly-ionized krypton. Astron Astrophys 2001;372:338–45.
[26] Mar S, Del Val JA, Rodríguez F, Peláez RJ, González VR, Gonzalo AB, et al. Measurement of transition probabilities in kr II UV and visible spectral lines. J Phys B: At Mol Opt Phys 2006;39(18):3709–21. doi:10.1088/0953-4075/39/18/001.
[27] Belmonte MT, Gavanski L, Peláez RJ, Aparicio JA, Djurović S, Mar S, et al. Kr II transition probability measurements for the UV spectral region. Mon Not R Astron Soc 2016;456(1):518–24. doi:10.1093/mnras/stv2710.
[28] Gigosos MA, Mar S, Perez C, de la Rosa MI. Experimental stark widths and shifts and transition probabilities of several xe II lines. Phys Rev E 1994;49(2).
[29] Del Val JA, Mar S, Gigosos MA, de la Rosa MI, Perez C, Gonzalez V. Design and characterization of a pulsed plasma source. Jpn J Appl Phys 1998;37:4177–81.
[30] Peláez RJ, Mar S, Aparicio JA, Belmonte MT, et al. Integration of an intensified charge-coupled device (ICCD) camera for accurate spectroscopic measurements. Appl Spectrosc 2012;66(8):970–8. doi:10.1366/12-06612.
[31] Aparicio JA, Pérez C, Del Val JA, Gigosos MA, De La Rosa MI, Mar S. Measurement of stark broadening and shift parameters of several ar i lines. J Phys B: At Mol Opt Phys 1998;31(22):4909–18. doi:10.1088/0953-4075/31/22/004.
[32] Thorne AP, Litzén U, Johansson S. Spectrophysics. Springer; 1999. ISBN 3-540-65117-9.
[33] Griem HR. Validity of local thermal equilibrium in plasma spectroscopy. Physical Review 1963;131(3):1170–6. doi:10.1103/PhysRev.131.1170.
[34] McWhirter RWP. Plasma diagnostic techniques. Huddlestone RH, Leonard SL, editors. Academic, New York; 1965.
[35] Travaillé G, Peyrusse O, Bousquet B, Canioni L, Pierres KML, Roy S. Local thermodynamic equilibrium and related metrological issues involving collisional-radiative model in laser-induced aluminum plasmas. Spectrochimica Acta - Part B Atomic Spectroscopy 2009;64(10):931–7. doi:10.1016/j.sab.2009.07.028.
[36] Djurović S, Peláez RJ, Cirisan M, Aparicio JA, Mar S. Stark widths of xe II lines in a pulsed plasma. J Phys B: At Mol Opt Phys 2006;39:2901–16.
[37] Bevington PR, Robinson DK. Data reduction and error analysis for physical sciences. third edition. McGraw-Hill; 2003. ISBN 0-07-247227-8.
[38] Sikstrom CM, Nilsson H, Litzen U, Blom A, Lundberg H. Uncertainty of oscillator strengths derived from lifetimes and branching fractions. J Quant Spectrosc Radiat Transfer 2002;74:355–68. doi:10.1016/S0022-4073(01)00258-8.
[39] Taylor BN, Kuyatt CE. Guidelines for evaluating and expressing the uncertainty of NIST measurement results - 1994 edition. 1994.
[40] Curry JJ, et al. Absolute transition probabilities for 559 strong lines of neutral cerium. J Phys D Appl Phys 2009;42. doi:10.1088/0022-3727/42/13/135205.
[41] Humphreys CJ. The third spectrum of krypton. Physical Review 1935;47:712–17.
[42] Cowley CR. The use of precision oscillator strengths as a means for obtaining large numbers of moderately accurate gf-values. Mon Not R Astron Soc 1983;202:417–25.
[43] Nitz DE, Curry JJ, Buuck M, Demann A, Mitchell N, Shull W, et al. Transition probabilities of ce i obtained from boltzmann analysis of visible and near-infrared emission spectra. J Phys B: At Mol Opt Phys 2018;51. doi:10.1088/1361-6455/aaa658.